Journal of Power Sources 207 (2012) 70–80

Contents lists available at SciVerse ScienceDirect

Journal of Power Sources

journal homepage: www.elsevier.com/locate/jpowsour

Estimating the thermal conductivity and diffusion coefficient of the microporous layer of polymer electrolyte membrane fuel cells

Nada Zamel*, Jürgen Becker, Andreas Wiegmann

Fraunhofer Institute for Industrial Mathematics (ITWM), Kaiserslautern, Germany

ARTICLE INFO

Article history:
Received 15 December 2011
Received in revised form 27 January 2012
Accepted 1 February 2012
Available online 9 February 2012

Keywords:
Microporous layer
Knudsen diffusion
Thermal conductivity
PEM fuel cells
Pore distribution

ABSTRACT

Investigation of the role in which the microporous layer (MPL) affects the overall diffusion of gases and conduction of heat in polymer electrolyte membrane (PEM) fuel cells is of great interest. In this study, we used stochastic models to generate a three-dimensional reconstruction of the MPL. This work is a continuation of the methods presented in [10]. A parametric study was carried out to investigate the effects of the MPL structure and MPL porosity on its diffusion coefficient and thermal conductivity. It was found that increasing the volume of the small pores of the MPL while keeping its overall porosity constant results in an increase in the Knudsen diffusion; hence a decrease of the overall diffusion coefficient. This similar trend is observed again once the porosity of the MPL is decreased. An increase in the volume of small pores also resulted in an increase of the thermal conductivity of the MPL. The parametric study was also extended to understand the effect of applying the MPL onto the gas diffusion layer (GDL). In this case, we investigated the effect of MPL thickness, porosity and its penetration into the GDL. The effect of the thickness on the thermal conductivity and diffusion coefficient of an MPL/GDL assembly can be explained using a resistance network. An increase in the penetration depth of the MPL results in an increase of the thermal conductivity and a decrease of the diffusion coefficient.

1. Introduction

The microporous layer (MPL) is a layer composed of carbon agglomerates, which is applied to the interface between the gas diffusion layer (GDL) and the catalyst layer (CL) of polymer electrolyte membrane (PEM) fuel cells. This layer is used to achieve a smooth, continuous interface between the GDL and the CL. The MPL consists of a powdery mixture of carbon black and PTFE particles, is sprayed onto the GDL and then sintered so the PTFE can bind the powder together. Experimental and numerical investigations have revealed that the performance of the cell is improved with the use of the MPL and much work is dedicated to understand the mechanisms in which the MPL enhances the performance.

One of the main mechanisms in which the MPL affects the overall performance of the cell is through assisting with liquid water management. This phenomenon has been studied numerically in [1,2], where in both studies, a two phase model was used to investigate the effects of placing a microporous layer at the cathode side. The results indicate that the MPL reduces the overall water flux to the cathode GDL particularly when the liquid water saturations are high; hence, improving membrane hydration and reducing the probability of GDL flooding. The reduction in the water flux towards the cathode side is mainly due to the increased tendency of the water to flow towards the anode. In other words, the presence of an MPL at the cathode side helps in establishing another route for liquid water removal from the cell. However, this trend is not observed when placing the MPL at the anode side only as Weber and Newman reported in [1]. From their findings, they suggested that the MPL improves the performance of the cell due to the following reasons:

1. The addition of the microporous layer reduces the ohmic losses in the fuel cell. This is mainly attributed to the enhanced hydration of the electrolyte membrane and the reduction of the overall resistance between the GDL and the CL.
2. The MPL reduces liquid water flooding in the GDL; hence, the transport of gaseous species is enhanced and the mass-transport limitations are minimized.
3. The MPL is a region that enhances the chemical and mechanical stability of the CL and the membrane. During compression, without the MPL, the catalyst layer may become entrenched into the GDL; hence, hindering its overall activity and accessibility. Similarly, during compression, the GDL may pierce the membrane resulting in reactant crossover.

* Corresponding author.
E-mail address: nada.zamel@gmail.com (N. Zamel).

0378-7753/$ – see front matter © 2012 Elsevier B.V. All rights reserved.
doi:10.1016/j.jpowsour.2012.02.003

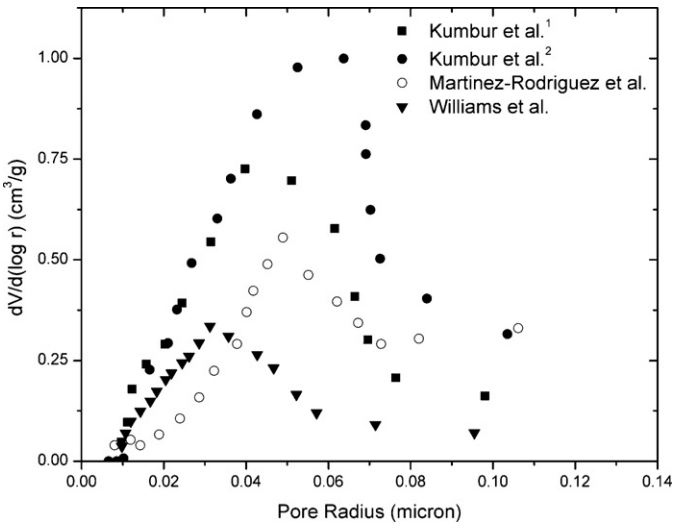

Fig. 1. Pore distribution of various microporous layers – data extracted from [3–6].

1.1. Structure

The structure of the MPL is complicated in that the distribution of the carbon agglomerates highly depends on the manufacturing and heat treatment processes, which directly affect the pore distribution of the MPL as is evident by Fig. 1. The data presented in this figure has been extracted from [3–6]. Kumbur et al. [3,4] evaluated the pore distribution for SGL 24DC and SGL 24BC. One of the main contributors to the differences between these two SGL carbon papers could be associated with the amount of PTFE used to treat the MPL. SGL 24DC contains more PTFE than SGL 24BC. The MPL measured by Martinez-Rodriguez et al. [5] was measured for an MPL applied to a TORAY TGP-H-060 with 10 wt.% PTFE. Finally, Williams et al. [6] investigated the pore distribution of SGL 10BB carbon paper. Although the MPL measured in [6] and in [3,4] are both SGL carbon papers, their manufacturing process may differ and their total thicknesses differ. The differences in weight and thickness of the carbon paper are of significance since the pore volume presented in all the studies is normalized by these two properties.

The effect of the manufacturing and application processes on the structure of the MPL onto the carbon paper GDL has been investigated by Chen et al. [7]. In their study, they examined the effect of two preparation methods, dry and wet layering of the MPL. The main differences between these two processes are the preparation of the carbon composite paste and the heat treatment process. From the findings of their investigation, they reported visual differences in the resultant MPL, which in turn significantly affected the overall performance of the cell.

It is clear that the impact of the MPL on the overall performance of the cell is positive. However, more insight into the mechanisms behind this effect is still needed and numerical simulation is often used to visualize the MPL's local impact. To do so, accurate transport properties are crucial for the numerical simulation in order to ensure its accuracy. Hence, estimation of the transport properties of the MPL have been the focus of many studies as discussed in the following section.

1.2. Properties of the MPL

1.2.1. Diffusion coefficient

The diffusion coefficient of the microporous layer is essential for simulating gas transport in the layer and experimental properties of this property can be found in literature. As the microporous layer cannot be found as a stand-alone layer, it is applied to one side of the carbon paper GDL and measurements are made for an MPL/GDL assembly. Thus, the change in diffusion coefficient due to the addition of an MPL is often reported in literature. LaManna and Kandlikar [8], measured the effect of the MPL on three SGL carbon paper electrodes. They found that the presence of the MPL reduces the overall through-plane diffusion coefficient of the electrode by 39%. Chan et al. [9] also measured the effect of the MPL on the through-plane diffusion coefficient of SolviCore carbon paper using a Loschmidt cell apparatus. In their study, they used a resistance network analysis to obtain the diffusion coefficient of an oxygen–nitrogen mixture through the microporous layer and estimated it as $1.54 \pm 0.22 \times 10^{-6}\ m^2\ s^{-1}$ for a calculated porosity value of 64%.

Numerically, Becker et al. [10] developed a mathematical formulation to take into account the Knudsen diffusion in the small pores of the MPL. They showed that in the presence of the MPL, the diffusion coefficient in both the in- and through-plane directions decreases. The decrease in the in-plane direction, however, was not as pronounced. Further, they found that the change in the diffusion coefficient is highly dependent on the overall penetration of the MPL into the carbon paper GDL. Numerical estimations of this nature are of importance since much about the structure of the MPL is unknown or is very difficult to measure.

1.2.2. Thermal conductivity

Estimation of the thermal conductivity of the microporous layer in the literature has recently gained interest. Using the guarded heat method, Karimi et al. [11] reported the through-plane thermal conductivity of the MPL at 70 °C and for various compression pressures. For SolviCore carbon paper with an MPL and 30% wet proofing, they found the thermal conductivity to lay in the range 0.25–0.52 $W\,K^{-1}\,m$ for a compression force of 0.7–13.8 bar. The in-plane thermal conductivity of this SolviCore paper was later measured by the same group [12] and reported as 3.87 $W\,K^{-1}\,m$. Burheim et al. [13] measured the through-plane thermal conductivity of an MPL-electrolyte membrane assembly. From these measurements, they estimated the thermal conductivity of the MPL to be 0.6 $W\,K^{-1}\,m$. The thermal conductivity of the MPL was also measured by Unsworth et al. [14]. They used the measured thermal conductivity of a bare carbon paper and a carbon paper/MPL assembly to isolate the contribution of the MPL. They estimated the thermal conductivity of the MPL to be 0.30 $W\,K^{-1}\,m$. They also found that the effect of the MPL on the through-plane thermal conductivity of the electrode highly depends on the amount of compression pressure applied to the electrode. As the compression pressure increases, the effect of the MPL on the thermal conductivity becomes negative. With this finding, they concluded that unlike carbon paper, the structure of the MPL does not change due to compression. Hence, the overall thermal conductivity of the MPL does not change with compression. Under compression, however, the contact between the carbon fibers in the carbon paper increases and its thermal conductivity increases; thus, at these conditions, the MPL acts as a thermal resistor and decreases the overall thermal conductivity of the backing layer.

In their study, Burlatsky et al. [15] reported their internal measurements of the thermal conductivity of the MPL as a stand alone layer. The measurements reported show that the thermal conductivity of an MPL/GDL assembly is much lower than that of a GDL only. They also showed that the measurements varied depending on the measurement technique. For instance, the thermal conductivity of a thin MPL with low and high Teflon content was 0.035 and 0.057 $W\,K^{-1}\,m$, respectively, using the laser flash method. However, with the modified substrate method, the value reported was not affected by the Teflon content and it was reported to be 0.097 $W\,K^{-1}\,m$. Comparing the two methods, one can see there

is much variation depending on the method. Specific conclusions about this study cannot be drawn as much information surrounding the experimental apparatus and experimental conditions is uncertain.

The thermal conductivity of the MPL was also reported theoretically in literature. In their model, Kang and Ju [16] analyzed the effects of the microporous layer on the transport mechanisms in PEM fuel cells. In their study, they assumed the thermal conductivity of the MPL to be $1.0\,W\,K^{-1}\,m$.

As can be seen, published data of the thermal conductivity of the MPL vary tremendously and are affected by the method of measurement. This variation coupled with limited knowledge in regards to the carbon used in the manufacture of the MPL makes it difficult to judge its thermal conductivity. Hence, in this study, we investigate the effect of the agglomerate structure on the thermal conductivity.

1.2.3. Electrical conductivity

Similarly to the diffusion coefficient and the thermal conductivity, the electrical conductivity of the MPL is measured based on the change in the overall electrical conductivity of the MPL/carbon paper assembly in comparison to that of the bare carbon paper. Experimental measurements of the electrical conductivity of the backing layer in the presence of the MPL are scarce. Ismail et al. [17] reported the contact resistance between the porous layer and the test rig in the presence of the MPL. They showed that the contact electrical resistance in the presence of the MPL decreases with the highest change observed was an increase by 40% in the overall contact resistance. The change in the in-plane electrical conductivity in the presence of the MPL was reported by Williams et al. [6] where they found the in-plane conductivity to increase by 4%. This small change in comparison to its through-plane counterpart suggests that the conduction of the electrons in the in-plane direction via the carbon fibers is efficient.

1.2.4. Intrinsic permeability

The intrinsic and relative permeability can be used as another measure to understand the effect of the MPL on the transport of the gas in the electrode. Again, due to the difficulty of separating the microporous layer from the carbon paper, the permeability of the bare carbon paper is first measured and then the permeability of the carbon paper/MPL assembly is measured. Hence, one can obtain an estimation of the effect of the MPL on this property. The through-plane intrinsic permeability of SGL 10BA (bare) and SGL 10BB (with MPL) was measured by Williams et al. [6]. In their study, they reported the intrinsic permeability to decrease from $3.1 \times 10^{-11}\,m^2$ to $5.8 \times 10^{-13}\,m^2$; a decrease of about 2 orders of magnitude. The hinderance of the permeability in the through-plane direction is mainly attributed to the small pores present in the MPL and the introduction of the Knudsen flow. The same trend is observed by Ihonen et al. [18] where they reported the through- and in-plane intrinsic permeability of SGL 10BA (bare) and SGL 10BC (with MPL). The in- and through-plane permeability of SGL 10BA was measured as 3.3×10^{-11} and $1.8 \times 10^{-11}\,m^2$, respectively and the in- and through-plane permeability of SGL 10BC was measured as 2.2×10^{-11} and $3.3 \times 10^{-13}\,m^2$, respectively. As expected, the change in the in-plane permeability due to the presence of the MPL is not as pronounced as its through-plane counterpart, which is mainly due to the availability of the pore space in the carbon paper GDL in the in-plane direction for fluid transport.

1.2.5. Capillary pressure

The capillary pressure is a measure for understanding liquid water transport in the porous material. Using the method of standard porosimetry, Kumbur et al. [3,4,19] measured the capillary pressure for SGL 24 series with an MPL and proposed a correlation for the capillary pressure based on the compression level, PTFE content and temperature. However, in their work, they did not separate the effect of the MPL from that of the carbon paper GDL as they did not measure the capillary pressure for a bare carbon paper. Hence, a full understanding of the effect of the MPL on the overall capillary pressure could not be obtained. In the study by Gostick et al. [20], the authors measured the capillary pressure of SGL 10BA (bare) and SGL 10BB (with MPL) and were able to isolate the effect of the MPL on the capillary pressure. Their finding is interesting as it suggests that the MPL plays a significant role in controlling liquid water levels in the GDL. They used this finding to further analyze the effect of the MPL on the capillary pressure in [21]. They showed that the liquid water saturation at the breakthrough pressure drops by 3% in the presence of the MPL. This suggests that a lower liquid water saturation level would be present in the porous electrode and the MPL plays a crucial role in water management of the cell.

As can be seen, much experimental work has been done to estimate the properties of the MPL. However, due to the uncertainty related to the structure of the MPL, it is difficult to obtain a comprehensive understanding of these properties. In this study, we estimate the diffusion coefficient and thermal conductivity of the microporous layer numerically using a three-dimensional reconstruction of the layer. We examine the effect of the following parameters on the transport properties:

- Effect of MPL porosity – experimentally, it is difficult to accurately measure the porosity of the MPL due to its penetration into the GDL. Efforts have been made to estimate this value as seen in [9,20].
- Effect of MPL thickness – in reality, the thickness of the MPL varies depending on the sample under study as has recently been reported by [9].
- Effect of MPL penetration – the penetration thickness of the MPL has a direct effect on the overall porosity of the electrode; hence, it affects the contact area between the carbon fibers of the GDL.

2. Structures

For common GDL and MPL materials, the pore sizes of MPL and GDL differ by more than two orders of magnitude. This implies, that a pore-scale model (with a number of grid points manageable by the subsequent numerical simulations) cannot at the same time show a representative part of the GDL and resolve the pores of the MPL. Therefore, we follow the approach taken in [10] and create two different structure models. First, a high-resolution model which only shows the pore structure of the MPL. Second, a low-resolution model showing the whole thickness of the GDL, where the MPL is added as homogenized porous medium.

In both cases, the structure models are created by stochastic methods. This means, that fibers or particles are distributed randomly in a predefined volume. These objects are then used to create the voxel mesh, which serves as mesh for the numerical simulations.

2.1. MPL

The three dimensional structure of the reconstructed MPL is given in Fig. 2. Scanning electron microscope (SEM) images (see e.g. Fig. 3b or [10,22]) show that the MPL consists of carbon particles which are – roughly – of spherical shape and equal size. These particles are not evenly distributed, but form a complicated network of large pores and agglomerates. This observations motivated the following construction algorithm, which is also illustrated in Fig. 4:

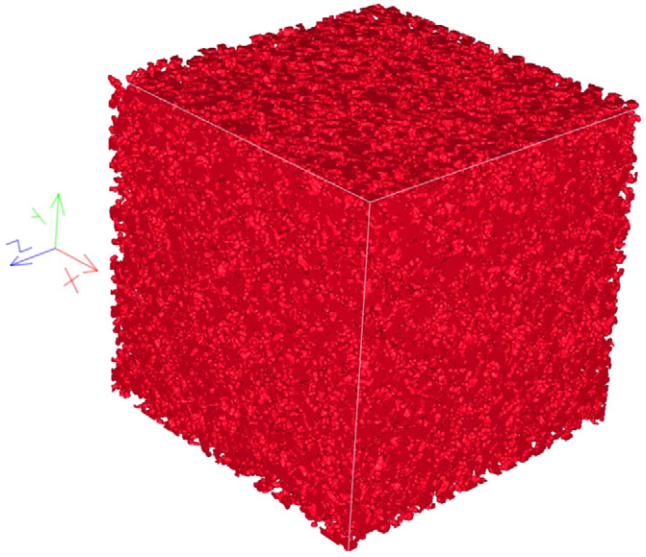

Fig. 2. Three dimensional reconstruction of the microporous layer.

- In a first step, part of the volume is set aside for the large pores. This is done by randomly distributing large spheres, which are allowed to overlap.
- In the second step, the carbon particles are created by distributing small spheres, which are again allowed to overlap with each other. In this step, the centers of the small spheres are not allowed to be inside one of the large spheres of the previous step.
- In the third and last step, the small particles are glued together by filling the small pores in between them.

This basically allows to change 5 parameters: In the first step, the diameter d_{pore} of the spheres and the volume fraction η_{pore} filled by them. In the second step, the diameter d_{particle} of the spheres and the volume fraction $\eta_{\text{particles}}$ filled by them. In the third step, the maximum pore diameter d_{fill} to be filled.

In this study, the parameters $d_{\text{particle}} = 40\,\text{nm}$ and $d_{\text{fill}} = 20\,\text{nm}$ were kept fixed while the others were varied. All MPL models used had a domain size of $(3\,\mu\text{m})^3$, consisting of 600^3 cubic voxels with a voxel length of 5 nm.

2.2. GDL

Following the ideas in [10,23], a GDL similar to a Toray paper can be modeled by straight, unbounded fibers with a circular cross section of 7 μm. For the GDL model used in this study, the fiber positions and directions were found by a Poisson line process with an orientation tensor of

$$\begin{pmatrix} 0.499975 & 0 & 0 \\ 0 & 0.499975 & 0 \\ 0 & 0 & 0.00005 \end{pmatrix}, \tag{1}$$

i.e. fibers are mainly oriented in the xy-plane (in-plane). Fibers were added to the structure until a porosity of 90% was reached. As gas diffusion layers contain both fibers and binder, 50 wt.% binder were added to the structure using the method described in [24], where it is assumed that the binder basically behaves like a wetting fluid and fills the smaller pores. The resulting GDL models thus have an overall porosity of 80%.

The GDL models used in this study had a domain size of $512\,\mu\text{m} \times 512\,\mu\text{m} \times 256\,\mu\text{m}$, consisting of $512 \times 512 \times 256$ cubic voxels with a voxel length of $1.0\,\mu\text{m}$.

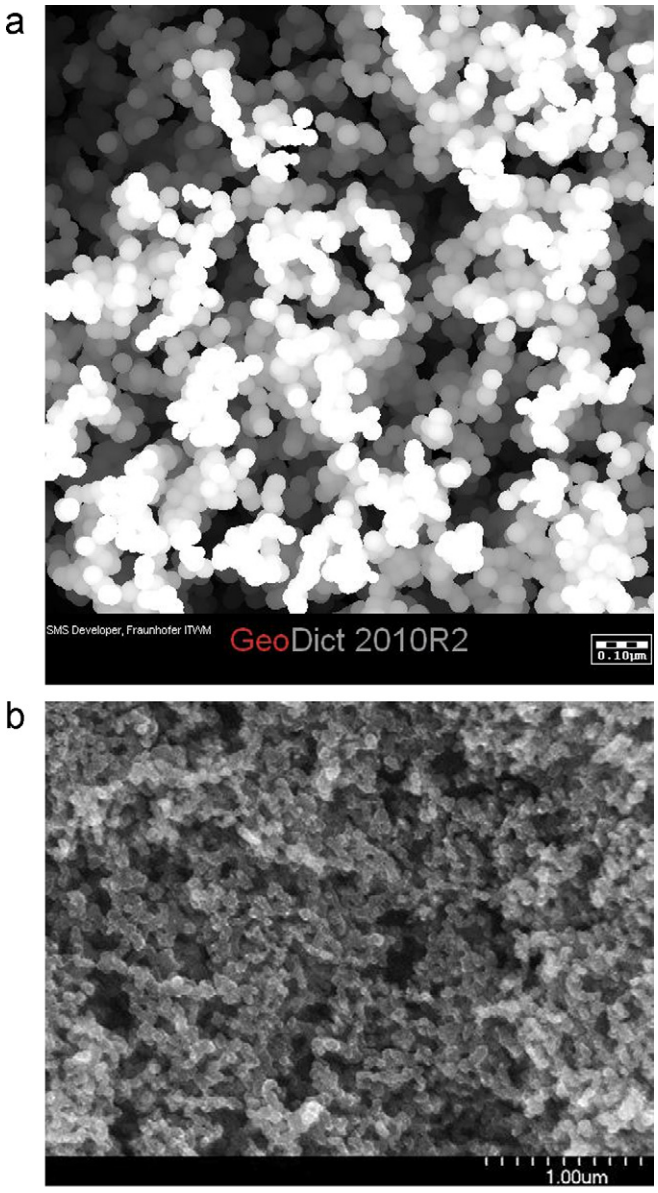

Fig. 3. (a) Cross-section of the reconstructed microporous layer; (b) SEM image of a microporous layer [22].

2.3. GDL/MPL assembly

The MPL is added to the GDL model as a homogenized porous layer. Thus, a voxel in the resulting mesh represents either solid (fibers or binder), void (GDL pores) or porous material (MPL) and the computational domain Ω subdivides into

$$\Omega = \Omega_{\text{solid}} \cup \Omega_{\text{void}} \cup \Omega_{\text{porous}}. \tag{2}$$

Fig. 5 illustrates one of the resulting structure models. The combined GDL/MPL models have the same resolution/voxel length as the GDL models. The domain size is $512\,\mu\text{m} \times 512\,\mu\text{m}$ in the xy-plane and 256 μm plus MPL thickness in the through-plane (z) direction. In this study, we vary the MPL thickness and penetration depth.

Fig. 4. Illustration of the MPL reconstruction algorithm.

3. Property calculation

The generated 3D voxel meshes are used to calculate the effective properties of the porous layer. Here, we consider pore size distribution, thermal conductivity and diffusivity.

At first, we determine the properties of the MPL using an MPL structure model. The resulting properties then enter into the simulation of the GDL/MPL assembly: As the MPL is not resolved on this scale, each voxel in Ω_{porous} represents a porous medium with the calculated effective properties. Of course, different MPL models result in different MPL properties which then will lead to different properties of the assembly.

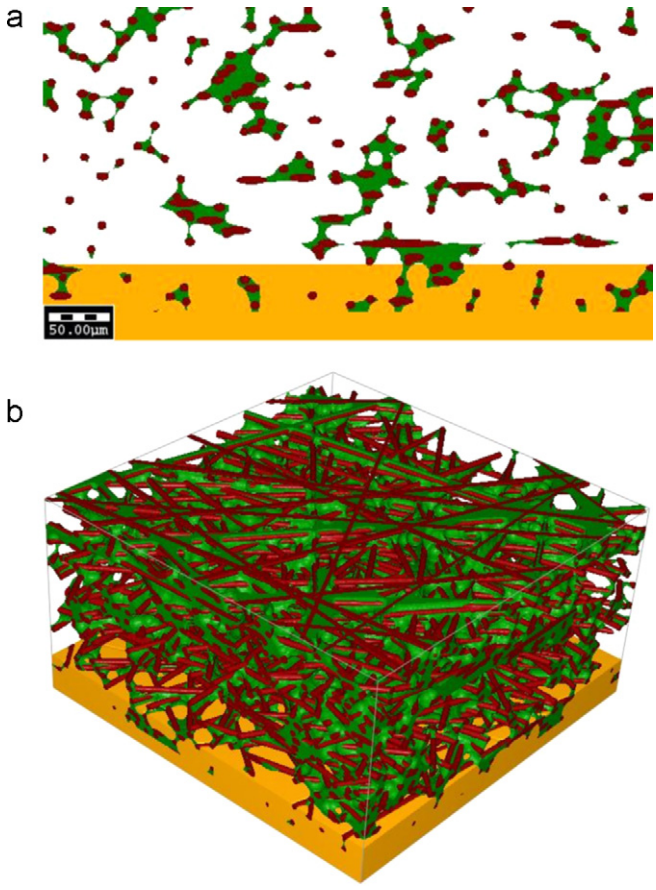

Fig. 5. A stack of the MPL and GDL (a) cross-section view; (b) 3-D view – MPL (yellow), binder (green), fibers (red), pores (white). (For interpretation of the references to color in this figure legend, the reader is referred to the web version of the article.)

3.1. Pore size distribution

The radius of a pore is defined by embedding spheres into the pore volume: a voxel belongs to a pore of radius r if r is the radius of the largest sphere, embedded in Ω_{pore}, containing this voxel. In this way, a radius is assigned to each voxel and the pore size distribution shows the distribution of these radii.

3.2. Thermal conductivity

Heat transport through a porous medium is macroscopically described by Fourier's law of conduction

$$j = -k_{\text{eff}} \nabla T, \tag{3}$$

where j is the heat flux and ∇T is the temperature drop over the medium. In general, the medium may be anisotropic and the effective conductivity k_{eff} is a 3×3 matrix. Here, the MPL models are isotropic by construction and in this case, Eq. (3) holds for a scalar k_{eff}.

The conductivity k_{eff} can be determined numerically by solving the stationary heat equation

$$\nabla \cdot (k(x) \nabla T) = 0 \quad \text{in } \Omega \tag{4}$$

directly on the 3D structure model. Here, $k(x)$ is the local (isotropic) thermal conductivity, which was set to $k(x) = 0$ in Ω_{void} and

$k(x) = k_{\text{Carbon}}$ in Ω_{solid}. To solve (4), the EJ-Heat solver [26] implemented in GeoDict [25] was used.

The same methodology is used to find the thermal conductivity of the MPL/GDL assembly. In this case, the conduction of heat occurs in four distinct parts of the assembly: the binder of the GDL, the solid fraction of the GDL, the void region of the GDL and the MPL. Due to the differences in the scale of pores of the two layers, the true pore morphology of the MPL cannot be coupled with that of the GDL and the computed thermal conductivity of the MPL is used. Mathematically the heat conduction is represented by Eq. (4) with the thermal conductivity k varying as:

$$k(x) = \begin{cases} 0 & x \in \Omega_{\text{void}} \\ k_{\text{mpl}} & x \in \Omega_{\text{MPL}} \\ k_{\text{solid}} & x \in \Omega_{\text{solid}} \end{cases} \quad (5)$$

where we assume that the binder and solid fibers of the GDL are manufactured with the same material; hence, their thermal conductivity is equal.

3.3. Diffusion coefficient

In general, diffusion occurs due to collision of gas molecules with each other (bulk diffusion) and to collision with the pore walls (Knudsen diffusion). The contribution of each type of diffusion to the overall transport process is described by the Knudsen number Kn, which is defined through

$$Kn = \frac{\lambda}{l_c}, \quad (6)$$

where λ is the mean free path and l_c is the characteristic length of the porous media, e.g. the average pore diameter. Large Knudsen numbers $Kn \gg 1$ indicate that the pore sizes of the porous medium are much smaller than the mean free path of the gas and diffusion occurs in the form of Knudsen diffusion. Small Knudsen numbers $Kn \ll 1$ indicate that the pores of the porous medium are much larger than the mean free path of the gas and bulk diffusion occurs. In the intermediate range, both mechanisms have to be taken into account.

As the mean free path of gases is in the order of 100 nm, diffusion inside the GDL is dominated by bulk diffusion and the Knudsen diffusion can be neglected in this case. Inside the MPL, pore sizes are of the same order of magnitude as the mean free path. Therefore, both diffusion types have to be taken into account.

To determine the MPL diffusivity, we follow the method developed in [10], calculate Knudsen diffusivity D_{Kn} and bulk diffusivity D_{bulk} first and then make use of Bosanquet's formula [27]

$$D = (D_{\text{bulk}}^{-1} + D_{Kn}^{-1})^{-1} \quad (7)$$

to determine the overall diffusivity D.

We determine the Knudsen diffusivity from the displacement of the diffusing molecules:

$$D_{Kn} = \frac{\epsilon}{2t} E[(x_t - x_0)(x_t - x_0)^T]. \quad (8)$$

Here, $x_t - x_0$ is the displacement of a molecule at time t from its starting position x_0, ϵ denotes the porosity and $E[.]$ the expectation value. To determine the displacement of each molecule we apply the random walk method of Babovsky [28] (also described in [10]).

We find the bulk diffusivity with the classical continuum mechanics approach by solving Laplace's equation

$$-\Delta c = 0 \quad \text{in } \Omega_{\text{void}} \quad (9)$$

for the concentration c in the pore space. This solution gives us the total diffusion flux j and with Fick's law

$$j = -D_{\text{bulk}} \nabla c \quad (10)$$

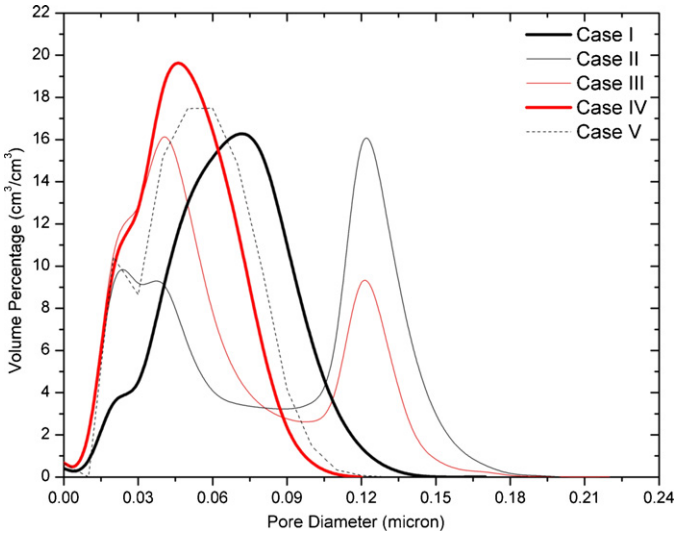

Fig. 6. Effect of pore density and diameter on the overall pore distribution of the microporous layer.

we determine D_{bulk}. To solve Eq. (9) numerically, we use GeoDict [25] and the underlying explicit jump finite volume solver [26]. The solver works directly on the voxel grid, so no re-meshing is needed. This enables us to find the solution fast and memory-efficient.

To determine the diffusivity of the GDL/MPL assembly, we have to solve

$$-\text{div}(D(x)\nabla c) = 0 \quad \text{in } \Omega \quad (11)$$

instead of Eq. (9), where the local diffusion coefficient $D(x)$ is given as

$$D(x) = \begin{cases} D_{\text{void}} & x \in \Omega_{\text{void}} \\ D_{\text{mpl}} & x \in \Omega_{\text{porous}} \\ 0 & x \in \Omega_{\text{solid}} \end{cases} \quad (12)$$

Here, D_{mpl} is the previously calculated diffusivity of the MPL and $D_{\text{void}} = (1/3)\lambda\bar{v}$ is the diffusion coefficient of the gas.

As mean free path λ we take 63.3 nm and as mean free velocity $\bar{v} = 425\ \text{m s}^{-1}$ [29]. To solve Eq. (11) numerically, we again use GeoDict [25] and the underlying solver [26].

4. Results and discussion

4.1. Effect of MPL structure

In this section, we investigate the effect of the MPL structure on its diffusion coefficient and thermal conductivity. Such an investigation is interesting due to the complications associated with the reproducibility of the structure of the MPL. In order to carry out this comparison, we vary the pore distribution of the MPL, keeping its overall porosity constant ~65%. Two parameters are varied, the initial pore size d_{pore} and their volume fraction η_{pore}. We investigate the following five cases:

1. Case I: $d_{\text{pore}} = 80$ nm, $\eta_{\text{pore}} = 80\%$
2. Case II: $d_{\text{pore}} = 160$ nm, $\eta_{\text{pore}} = 40\%$.
3. Case III: $d_{\text{pore}} = 160$ nm, $\eta_{\text{pore}} = 20\%$.
4. Case IV: $d_{\text{pore}} = 80$ nm, $\eta_{\text{pore}} = 20\%$.
5. Case V: $d_{\text{pore}} = 80$ nm, $\eta_{\text{pore}} = 40\%$.

The pore size distribution of these models is given in Fig. 6. Increasing the initial diameter of the pores (i.e. Cases II and III) results in a more densely packed structure. This is observed by the formation of small pores. Decreasing the initial solid fraction results

Table 1
Effect of structure on the thermal conductivity and diffusion coefficient of the MPL.

Case	Thermal conductivity	Diffusion coefficient ($\times 10^{-6}$ m^2 s^{-1})	Diffusivity $\left(Q = \frac{D_{eff}}{D_{bulk}}\right)$ [a]
I	0.094	1.92	0.106
II	0.120	1.78	0.099
III	0.104	1.65	0.092
IV	0.092	1.59	0.088
V	0.095	1.67	0.093

[a] The bulk diffusion coefficient is estimated at 0 °C to be 1.8×10^{-5} m^2 s^{-1}.

in shifting the pore distribution to the left; in other words, the overall size of the pores decreases. The effect of these two parameters on the thermal conductivity and diffusion coefficient are calculated as given in Table 1. The results show that the effect of the structure on the overall thermal conductivity and diffusion coefficient is minimal. For Cases II and III, the thermal conductivity is slightly higher than the base case (Case I) due to the more packed agglomerates. Similarly, their diffusion coefficient is lower due to the higher contribution of the Knudsen diffusion to the overall diffusion coefficient. The smaller pore sizes are also the main contributor to the decrease of the overall diffusion coefficient of Cases IV and V.

In the next sections of this paper, the MPL under investigation is that described by Case I. The pore distribution of this structure and its diffusion coefficient compare very well with experimental data.

4.2. Pore distribution of the microporous layer

The pore distribution of the reconstructed MPL is given in Fig. 7 and compared against published experimental data. As it can be seen, the overall trend of the pore distribution is similar in both cases. The radius of the pores of the reconstructed MPL lies in the range $0.01 \leq r \leq 0.085$ μm with the peak occurring at a radius of 0.04 μm. The main discrepancy between the numerical and experimental values is the actual height of the curve. This is explained by the fact that the experimental data was obtained for an MPL applied onto carbon paper and normalized using the total weight of the GDL/MPL assembly, which is much higher than that of the MPL. The numerical results on the other hand are obtained for the MPL only.

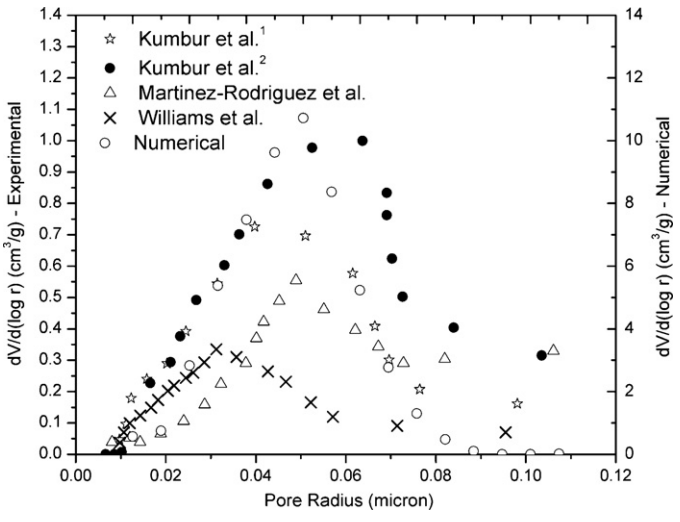

Fig. 7. Comparison of the pore distribution of the reconstructed MPL with experimental data – the porosity of the reconstructed MPL is 70%.

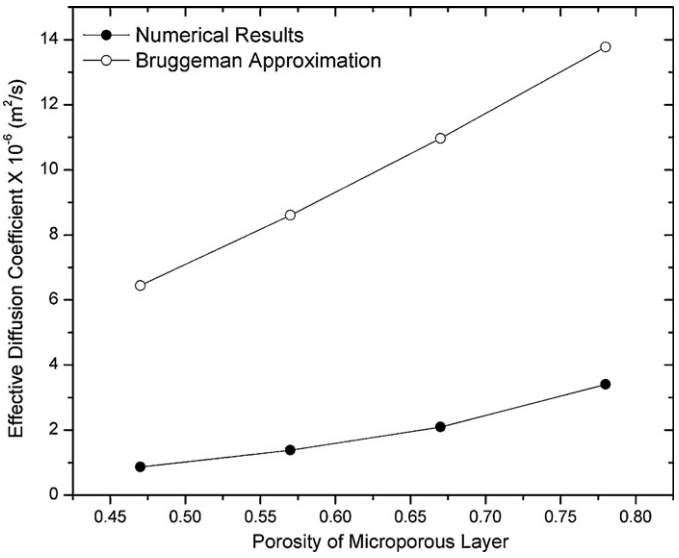

Fig. 8. Diffusion coefficient – Bruggeman Approximation: $D_{eff} = D_{bulk}(\epsilon)^{1.5}$.

4.3. Properties of the microporous layer

For the purpose of simulating the transport phenomena in PEM fuel cells, the MPL is often treated as a stand-alone domain and all the conservation equations must be resolved in this domain. Using the macro-homogeneous assumption, the solid and void regions of this layer are lumped together and the so-called effective properties are used. In the current literature, the Bruggeman approximation is often utilized to estimate the diffusion coefficient and the thermal conductivity of this layer. However, as illustrated in Figs. 8 and 9, this approximation does not accurately predict these properties. The Bruggeman Approximation overestimates the diffusion coefficient of the MPL due to the fact that the Bruggeman formula neglects the Knudsen effect. However, the Knudsen effect should not be neglected when the pore size is as small as one micrometer and it usually becomes dominant when the pore size is less than 100 nm, which is the case for the MPL. The difference between the numerical results of the thermal conductivity and those predicted by the Bruggeman Approximation arises from the difference in structure. The Bruggeman formula was derived for closely packed

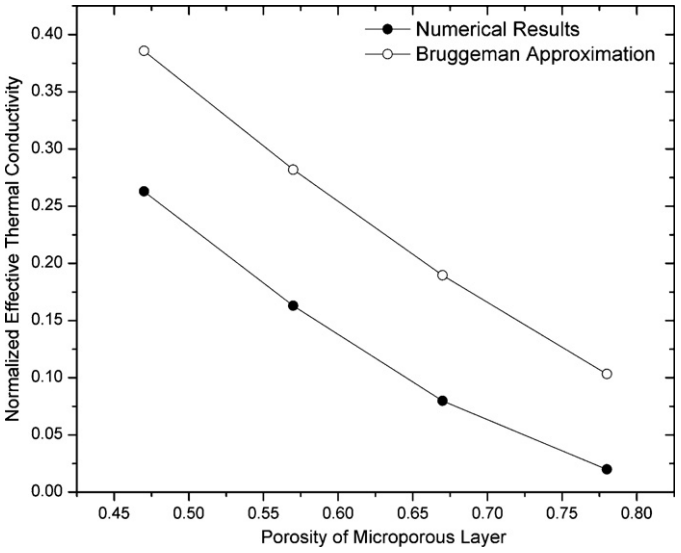

Fig. 9. Thermal conductivity – Bruggeman approximation: $\frac{k_{eff}}{k_{solid}} = (1-\epsilon)^{1.5}$.

spherical particles whereas in the case of the MPL, neighboring agglomerates might not have perfect contact. In other words, the contact resistance between the spherical agglomerates is different in this study than that considered by Bruggeman [30].

As the porosity of the microporous layer directly depends on the packing of the agglomerates and the MPL is usually attached to the carbon paper, obtaining its physical porosity could be difficult. Experimentally, two porosity values have been reported [20,9]. These values are estimated values based on the estimated penetration and thickness of the layer and the pore volume of the substrate. Gostick et al. [20] suggested that a correlation between the pore volume and the thickness of the layers can be used to estimate the porosity of the MPL as follows:

$$\epsilon_{\mathrm{MPL}} = (1-\phi)\epsilon_T \frac{t_T}{t_{\mathrm{MPL}}} \tag{13}$$

where ϵ_{MPL} is the porosity of the MPL, ϕ is the proportion of the total pore volume in the portion of the electrode not intruded by the MPL material and is found using curve fits of the capillary pressure, ϵ_T is the total porosity of the electrode, t_T is the total thickness of the electrode and t_{MPL} is the thickness of the MPL.

Using Eq. (13), Gostick et al. [20] estimated the porosity of an MPL on an SGL 10BB to be 72% and Chan et al. [9] estimated the porosity of an MPL applied onto SolviCore carbon paper to be 64%. The variation of the porosity reported by the two studies could be associated with experimental errors as well as differences in structure. As mentioned earlier in the introduction section, Chan et al. [9], measured the diffusion coefficient of the MPL to be $1.54 \pm 0.21 \times 10^{-6}\ \mathrm{m^2\ s^{-1}}$, which translates to a diffusivity, Q, ($Q = D_{\mathrm{eff}}/D_{\mathrm{bulk}}$) of 0.073 ± 0.01. At a porosity value of 65%, the numerical estimation of the diffusivity of an oxygen–nitrogen mixture is 0.106. The difference between the numerical estimation of this study and the experimentally measured diffusion coefficient can be attributed to the method of estimation utilized in [9]. As mentioned earlier, the MPL cannot be found as a stand alone layer; hence, the diffusion coefficient measurements are done using a GDL/MPL assembly. In [9], the authors used a series network resistance to estimate the diffusion coefficient of the MPL. Due to uncertainties surrounding the penetration of the MPL into this GDL, this method does not take into account the resistance to diffusion due to this penetration. Hence, the diffusion coefficient of the MPL can be underestimated.

As mentioned in the introduction section of this study, the thermal conductivity of the MPL has been measured experimentally and discrepancy between these measurements is apparent. This discrepancy can be the result of various reasons with the most significant being differences in the actual contact area between the spherical agglomerates. In the MPL, micro-cracks could be present due to the manufacturing process. These cracks can result in a decrease in contact area; hence, an increase in thermal resistance and a decrease in the overall thermal conductivity. Further, examining the thermal conductivity (of a SolviCore MPL) measured by Burheim et al. [13] and Unsworth et al. [14] another reason for this difference can be speculated. This difference can be attributed to the amount of PTFE added in the production of the MPL. Exact information in regards to this amount is not available. In their study Unsworth et al. [14] estimated the amount of PTFE in the MPL to be approximately 30%.

In order to compare the numerical results of this study to the experimental measurements of the thermal conductivity of the MPL, one needs the bulk thermal conductivity of the carbon material used for the manufacturing of the MPL. The assumption that the carbon of the microporous layer is the same as that of the GDL could be questionable. This is so since the properties of the carbon are very much affected by the heat treatment of this layer during manufacturing. Further, the addition of PTFE can significantly reduce the bulk thermal conductivity of the agglomerates. The thermal conductivity of the MPL is 3 orders of magnitude lower than that of carbon (see [31,32]). Comparing our numerical result in this study to the measurements of [13,14], the bulk conductivity would be estimated in the range of $3–6\ \mathrm{W\,K^{-1}\,m}$.

4.4. Properties of the GDL/MPL assembly

In this section, the effect of the MPL on the overall properties of the electrode is investigated. As mentioned earlier, the properties of the MPL are first resolved and then the MPL is added as a homogenized layer in the electrode and the overall diffusion coefficient and thermal conductivity of the electrode are then estimated. In this section, we investigate the effect of thickness, porosity and penetration of the MPL on the properties. The properties used for the MPL under this section are those of Case I described earlier.

The penetration of the MPL into the GDL is achieved by filling in the pore space of the GDL with the MPL material. In this case, the effective properties calculated for the MPL using its model are used to characterize the homogenized MPL material.

The penetration and thickness of the MPL are highly dependent on the manufacturing process of the MPL and the substrate on which it is applied. From experimental observations, these two parameters can highly vary. In Ref. [9], Chan et al. measured a varying thickness for the MPL depending on the substrate on which it is applied. An average thickness of 38.4 and 60.7 μm was measured for an MPL on SIGRACET 25 DC and SolviCore Type B, respectively. Further in Ref. [20], the thickness of the MPL (applied on an SGL carbon paper) has been estimated at about 118 μm with a penetration depth of 63 μm. In the following sections of this paper, our main objective is to numerically understand the effects of these two parameters.

4.4.1. Effect of thickness of the microporous layer

As mentioned earlier, the thickness of the microporous layer can vary tremendously; hence, it is interesting to investigate the effect of the thickness on the overall diffusion coefficient and thermal conductivity of the electrode. To carry out this investigation, the MPL porosity is kept constant at 65% for all thicknesses. The effect of the MPL thickness on the diffusion coefficient and the thermal conductivity is illustrated in Fig. 10. Due to the small diffusion coefficient of the MPL in comparison to the GDL, the overall diffusion coefficient of the electrode decreases in both directions (through- and in-plane). This implies that the small pores of the MPL create higher resistance for the diffusion and increasing the thickness of this layer will result in hindering the overall diffusion process. From Fig. 10, the effective diffusion coefficient of the electrode decreases with the increase of the MPL thickness. This implies that the resistance to diffusion due to the addition of the MPL increases with its thickness. However, this trend is not valid for the thermal conductivity. As it can be seen, the through-plane thermal conductivity increases with the increase of the thickness whereas its in-plane counterpart decreases. This is mainly due to the difference between the through- and in- plane thermal conductivities of the GDL. The through-plane thermal conductivity of the GDL is much lower than that of the MPL; hence, the addition of the MPL will enhance heat conduction in the through-plane direction. In the in-plane direction, the thermal conductivity of the GDL is much higher than the MPL; hence, the addition of the MPL will hinder heat conduction in the in-plane direction.

The observed trend can be explained from a resistance network perspective. In the through-plane direction, a series network governs heat conduction and mass diffusion whereas a parallel network can be used to analyze this transfer in the in-plane direction.

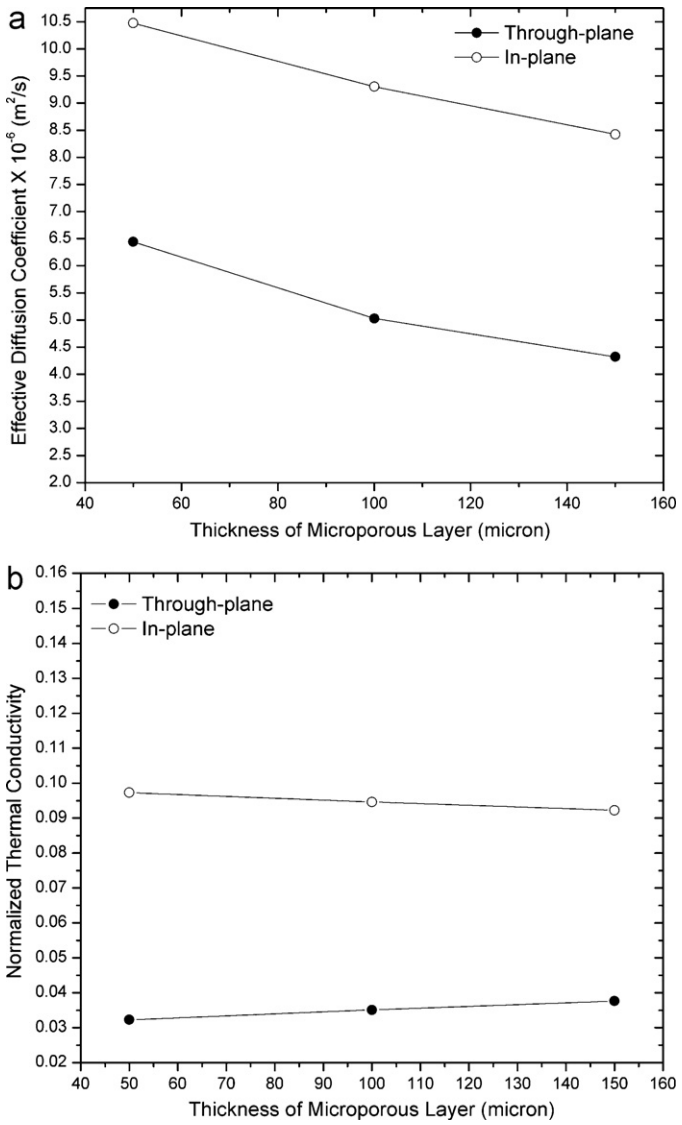

Fig. 10. Effect of the thickness of the MPL on the overall (a) diffusion coefficient; (b) thermal conductivity of the electrode.

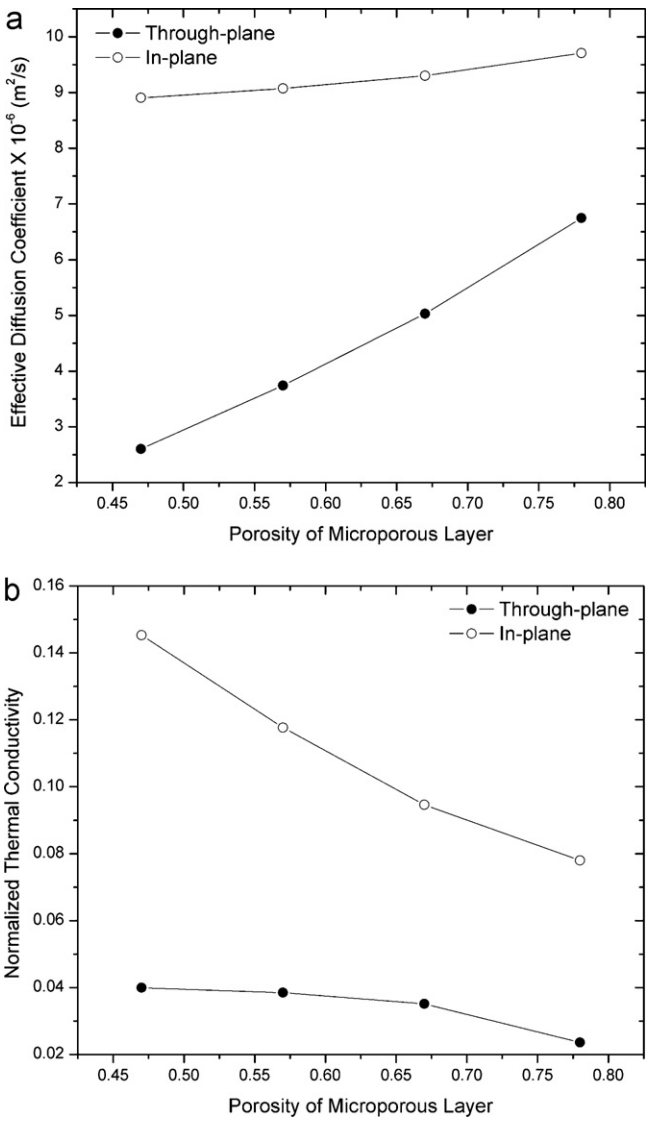

Fig. 11. Effect of the porosity of the MPL on the overall (a) diffusion coefficient; (b) thermal conductivity of the electrode.

The resistance through each layer (GDL and MPL) can be written as:

$$R = \frac{L}{\xi A_c} \tag{14}$$

where L is the length scale through which the transfer occurs, ξ denotes the transport property and A_c is the cross-section area.

With this type of analysis, the through- and in-plane properties of the electrode can be obtained as:

$$\xi_{\text{total}} = \begin{cases} \dfrac{L_{\text{total}}}{(L_{\text{MPL}}/\xi_{\text{MPL}}) + (L_{\text{GDL}}/\xi_{\text{GDL}})} & \text{Through-plane} \\ \dfrac{\xi_{\text{MPL}} L_{\text{MPL}} + \xi_{\text{GDL}} L_{\text{GDL}}}{L_{\text{total}}} & \text{In-plane} \end{cases} \tag{15}$$

where the superscripts, total, MPL and GDL stand for the electrode, microporous layer and gas diffusion layer, respectively.

Fig. 10 also shows that the overall thermal conductivity of the electrode is higher than that of the GDL, whereas the diffusion coefficient is lower. This is the case since the thermal conductivity of the MPL is higher than that of the GDL and its diffusion coefficient is much lower. Hence, using this finding and Eq. (15), certain properties of the electrode under compression can be deduced. As discussed earlier in many studies [1], the MPL is very mechanically stable. Due to its tightly packed agglomerates, it does not deform under compression. Hence, under compression of the thermal conductivity of the electrode (GDL + MPL) would be lower than that of the bare GDL. This phenomenon is also easily observed from the experimental data reported by Karimi et al. [11]. Similarly, the diffusion coefficient of the electrode can become higher than that of the bare GDL after certain compression pressures.

4.4.2. *Effect of porosity of the microporous layer*

The porosity is a measure of the packing, or density, of the microporous layer. It is interesting to understand how the density of these agglomerates would affect the transport coefficients of the overall backing layer as is illustrated in Fig. 11. As the porosity of the MPL increases, the diffusion coefficient of the backing layer increases whereas the overall thermal conductivity decreases. The increase in the diffusion coefficient is attributed to the increased pore space in the MPL available for diffusion. At the same time, however, due to the decrease in packing density of the MPL, higher thermal resistances are introduced and the thermal conductivity of the overall backing layer is reduced.

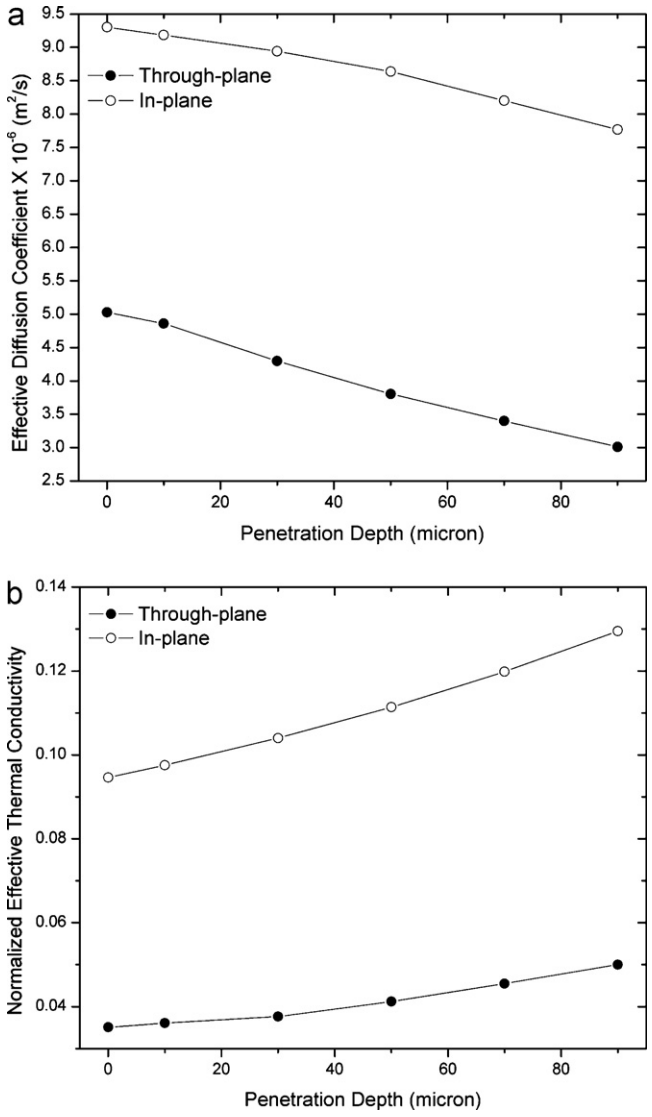

Fig. 12. Effect of the penetration depth of the MPL on the overall (a) diffusion coefficient; (b) thermal conductivity of the electrode.

4.4.3. Effect of MPL penetration

Due to the small size of the carbon agglomerates (dia. 40 (nm)) of the MPL, the penetration of the layer into the carbon paper is inevitable. The average pore diameter of the carbon paper GDL is much larger than the agglomerate diameter; hence, the carbon agglomerates will fill the pores of the GDL. The penetration depth of the MPL into the GDL relies heavily on the manufacturing process of the electrode. Due to this dependence, this depth varies tremendously and is sometimes difficult to accurately characterize experimentally. In this section, we study the effect of this parameter from a numerical perspective to gain a comprehensive understanding of its influence on the diffusion coefficient and the thermal conductivity of the porous electrode. The dependence of these two properties is found to be linear in both directions, through- and in-plane, as given by Fig. 12.

5. Conclusion

Interest in the microporous layer is mainly attributed to its ability to enhance the fuel cell performance. However, due to the complication associated with the separation of this layer from the backing layer, experimental measurements of its transport properties can be troublesome. Using stochastic methods to reconstruct the 3-D pore distribution, we were able to investigate the effect of the pore distribution on the transport properties (mainly diffusion coefficient and thermal conductivity) of the MPL. The estimated thermal conductivity and diffusion coefficient of the MPL were used to carry out a parametric study to investigate the effect of MPL porosity, thickness and penetration depth on the overall properties of an MPL/GDL assembly. Further, a detailed analysis of the differences between the numerically estimated properties of the MPL and published experimental measurements was put forward. Direct comparison between the numerical findings and published experimental data is quite difficult. The numerically estimated diffusion coefficient was found to be higher than that of experimental measurements. As experimental measurements neglect the penetration of the MPL into the GDL, they tend to underestimate the diffusion coefficient. The diffusibility of an MPL with a 65% porosity was estimated numerically as 0.106. In the case of the thermal conductivity, the numerical estimation of the normalized thermal conductivity along with the published experimental data were used to estimate the bulk thermal conductivity of the carbon agglomerates to be in the range of 3–6 $W K^{-1}$ m.

Acknowledgement

J. Becker gratefully acknowledges funding from the German Federal Ministry of Education and Research (BMBF) through the project PemCaD (Grant No. 03SF036OA).

References

[1] A.Z. Weber, J. Newman, Journal of the Electrochemical Society 152 (2005) A677–A688.
[2] U. Pasaogullari, C.Y. Wang, K.S. Chen, Journal of the Electrochemical Society 152 (2005) A1574–A1582.
[3] E.C. Kumbur, K.V. Sharp, M.M. Mench, Journal of the Electrochemical Society 154 (2007) B1295–B1304.
[4] E.C. Kumbur, K.V. Sharp, M.M. Mench, Journal of the Electrochemical Society 154 (2007) B1305–B1314.
[5] M.J. Martinez-Rodriguez, C. Tong, S. Shimpalee, J.W. Van, Zee, Electrochemical Society Meeting 33 (2010) 1133–1141.
[6] M.V. Williams, E. Begg, L. Bonville, H.R. Kunz, J.M. Fentona, Journal of the Electrochemical Society 151 (2004) A1173–A1180.
[7] J. Chen, H. Xu, H. Zhang, B. Yi, Journal of Power Sources 182 (2008) 531–539.
[8] J.M. LaManna, S.G. Kandlikar, International Journal of Hydrogen Energy 36 (2011) 5021–5029.
[9] C. Chan, N. Zamel, X. Li, J. Shen, Electrochimica Acta. doi:10.1016/j.electacta.2011.12.10.
[10] J. Becker, C. Wieser, S. Fell, K. Steiner, International Journal of Heat and Mass Transfer 54 (2011) 1360–1368.
[11] G. Karimi, X. Li, P. Teerstra, Electrochimica Acta 55 (2010) 1619–1625.
[12] P. Teerstra, G. Karimi, X. Li, Electrochimica Acta 56 (2011) 1670–1675.
[13] O. Burheim, P.J.S. Vie, J.G. Pharoah, S. Kjelstrup, Journal of Power Sources 195 (2010) 249–256.
[14] G. Unsworth, N. Zamel, X. Li, International Journal of Hydrogen Energy. doi:10.1016/j.ijhydene.2011.12.012.
[15] S.F. Burlatsky, W. Atrazhev, M. Gummalla, D.A. Condit, F. Liu, Journal of Power Sources 190 (2009) 485–492.
[16] K. Kang, H. Ju, Journal of Power Sources 194 (2009) 763–773.
[17] M.S. Ismail, T. Damjanovic, D.B. Ingham, M. Pourkashanian, A. Westwood, Journal of Power Sources 195 (2010) 2700–2708.
[18] J. Ihonen, M. Mikkola, G. Lindbergh, Journal of the Electrochemical Society 151 (2004) A1152–A1161.
[19] E.C. Kumbur, K.V. Sharp, M.M. Mench, Validated, Journal of the Electrochemical Society 154 (2007) B1315–B1324.
[20] J.T. Gostick, M.W. Fowler, M.A. Ioannidis, M.D. Pritzker, Y.M. Volfkovich, A. Sakars, Journal of Power Sources 156 (2006) 375–387.
[21] J.T. Gostick, M.A. Ioannidis, M.W. Fowler, M.D. Pritzker, Electrochemistry Communications 11 (2009) 576–579.
[22] J.H. Chun, K.T. Park, D.H. Jo, Y.J. Lee, et al., International Journal of Hydrogen Energy 35 (2010) 11148–11153.
[23] V.P. Schulz, P.P. Mukherjee, J. Becker, A. Wiegmann, C.Y. Wang, Journal of the Electrochemical Society 154 (2007) B419–B426.
[24] J. Becker, R. Flückiger, M. Reum, F.N. Büchi, F. Marone, M. Stampanoni, Journal of the Electrochemical Society 156 (2009) B1175–B1181.
[25] A. Wiegmann, et al., GeoDict Virtual Micro Structure Simulator and Material Property Predictor, 2001–2011. http://www.geodict.com.

[26] A. Wiegmann, A. Zemitis, EJ-HEAT: A Fast Explicit Jump Harmonic Averaging Solver for the Effective Heat Conductivity of Composite Materials, Technical Report 94, Fraunhofer ITWM Kaiserslautern, 2006.
[27] W.G. Pollard, R.D. Present, Physical Review 73 (1948) 762–774.
[28] H. Babovsky, Journal of Statistical Physics 44 (1986) 865–878.
[29] J.O. Hirschfelder, C.F. Curtiss, R.B. Bird, Molecular Theory of Gases and Liquids, John Wiley, New York, 1954.
[30] D.A.G. Bruggeman, Annalen der Physik (Leipzig) 24 (1935) 636–664.
[31] J. Blumm, A. Lindemann, M. Meyer, C. Strauser, Characterization of PTFE Using Advanced Thermal Analyses Technique, 2010. http://www.netzsch-thermal-analysis.com/download/P-022_315.pdf. NETZCH.
[32] R.A. Buerschaper, Journal of Applied Physics 15 (1944) 452–454.